Applied Physics Letters

Perspective on statistical effects in the adhesion of micropatterned surfaces

Cite as: Appl. Phys. Lett. **119**, 230502 (2021); https://doi.org/10.1063/5.0073181
Submitted: 28 September 2021 • Accepted: 20 November 2021 • Published Online: 07 December 2021

Jamie A. Booth and René Hensel

Applied Physics Letters PERSPECTIVE scitation.org/journal/apl

Perspective on statistical effects in the adhesion of micropatterned surfaces

Cite as: Appl. Phys. Lett. **119**, 230502 (2021); doi: 10.1063/5.0073181
Submitted: 28 September 2021 · Accepted: 20 November 2021 ·
Published Online: 7 December 2021

Jamie A. Booth[1,a] and René Hensel[2,a]

AFFILIATIONS

[1]Mechanical Engineering Department, California State University, Northridge California 91330, USA
[2]INM–Leibniz Institute for New Materials, Campus D2 2, 66123 Saarbrücken, Germany

[a]**Authors to whom correspondence should be addressed:** jamie.booth@csun.edu and rene.hensel@leibniz-inm.de

ABSTRACT

Bioinspired micropatterned adhesives have attracted extensive research interest in the past two decades. In modeling the performance of these adhesives, the common assumption has been that the adhesive strength of each sub-contact is identical. Recent experiments, however, have shown that interfacial defects of different characters lead to a distribution of the adhesive strength within a fibrillar array. Based on experimental observations of detachment events, a statistical model for the distribution of the local adhesive strength and the resulting performance of a micropatterned adhesive are presented. This approach constitutes a paradigm shift, providing better understanding of micropatterned adhesives under real conditions. Examples presented include the prediction of unstable detachments in compliant systems. Future directions are discussed, including the extension of the statistical approach to non-uniform loading and rate-dependent effects, the contribution of suction to adhesion and aging of contacts over specific time periods, as well as the necessity for a more in-depth understanding of defect formation considering surface roughness and other imperfections in the system.

I. INTRODUCTION

Exploiting mechanisms often inspired by nature, dedicated microstructure designs offer a promising approach for enabling new functionalities in emerging applications.[1] A prominent example is the fibrillar adhesive toe pad of many climbing animals such as beetles, spiders, and geckos.[2–4] As demonstrated by many previous studies (see, e.g., Refs. 5–8), splitting an adhesive pad into several individual fibrils offers several benefits to enable stronger and more reliable adhesive contacts. This insight has driven adoption of the concepts in numerous applications ranging from novel adhesive grippers for handling operations,[9,10] crawling, climbing, and soft robots,[11,12] docking mechanisms for space applications, skin adhesives for wound care and wearables,[13,14] and underwater adhesives.[15,16]

Most commonly, synthetic dry adhesives are comprised of arrays of fibrillar surface microstructures connected by a backing layer. Numerous analytical and numerical models have been developed to gain an insight into the underlying mechanisms[6,7,17–19] and optimize fibril designs.[20–23] Most early studies focused on individual fibrils, presuming that the adhesive forces can be summed to describe a complete fibrillar array. However, this requires an equal load distribution on all fibrils, and that all fibrillar sub-contacts have the same adhesive strength. These ideal conditions are scarcely attained in real applications. Theoretical models considering the total load capacity of fibrillar arrays have been developed in terms of uneven load distributions due to elastic coupling among fibrils,[24,25] misalignment,[26] surface curvature,[27,28] non-uniform height distributions,[18,29,30] and statistical strength distributions due to roughness and defects.[30] The latter has recently been validated by *in situ* observations of detachment processes and has led to a paradigm shift in the way adhesive arrays are understood through statistical characterization of the adhesive strength among subcontacts.[31–33] Most of these studies propose severe reductions in the total load capacity by more than half, which must be considered for creating reliable micropatterned adhesive systems used in real applications.

In the present Perspective, we aim to highlight the need for statistical models to provide a real-world characterization of the performance of micropatterned adhesives, beyond the common assumption of the uniform fibril strength within an array. Beginning with the behavior of individual fibrils, Sec. II presents proposed strategies for tuning interfacial stress distributions, as well as considering the sources and impact of interfacial defects on adhesive performance and experimental methods for observing

defect-controlled detachments. In Sec. III, we introduce statistical approaches to characterize adhesive strength distributions in micropatterned adhesive arrays. In Sec. IV, we show examples that demonstrate the benefit of using such statistical models to describe the performance of micropatterned arrays. Future directions and open tasks are finally discussed in Sec. V.

II. ADHESIVE STRENGTH AND DETECTION OF SUB-CONTACTS IN MICROPATTERNED ADHESIVES

The existence of intermolecular surface interactions and the generation of intimate contacts are necessary but not sufficient to ensure strong attachment in temporary bonding applications. The elastic nature of the bodies in contact leads to concentration of stress at characteristic geometric features, such as the contact edge, or at the tip of a defect within the contact. Since only a small region supports elevated stresses associated with bond rupture at any instant, the external load at which failure occurs is significantly reduced as compared to the situation in which the nominal stress across the entire contact could be raised to the level of the bond strength. Consequently, the design of micropatterned surfaces has been focused upon mitigation of these effects.

A. Dependence upon fibril geometry

The simplest geometry of a micropatterned sub-contact is the cylindrical punch, forming a circular contact with a defined contact edge [Fig. 1(a)]. A characteristic contact edge stress concentration is revealed, which is detrimental to the strength of attachment.[34,35] The strength (the critical value of the remote stress applied to the sub-contact) is obtained from linear elastic fracture mechanics for the case of an incompressible elastic punch and a rigid substrate (as is a good approximation in typical applications of elastomeric micropatterned adhesives)[35]

$$\sigma_{\max} = \frac{\alpha\sqrt{E^* W}}{l_e^{0.1} a^{0.4}}, \tag{1}$$

where Young's modulus is E, Poisson's ratio is ν, and $E^* = E/(1-\nu^2)$. The work of adhesion, characteristic of the intrinsic strength of the adhesive interaction, is W. The radius of the punch is a, and the characteristic size of a defect at the contact edge (assumed to be a small opening within the singular stress field, controlled by the radius of the curvature at the edge) is l_e. The constant α is of order unity. One apparent approach for increasing the strength of a sub-contact is to reduce the radius a, which eventually may lead to saturation of the

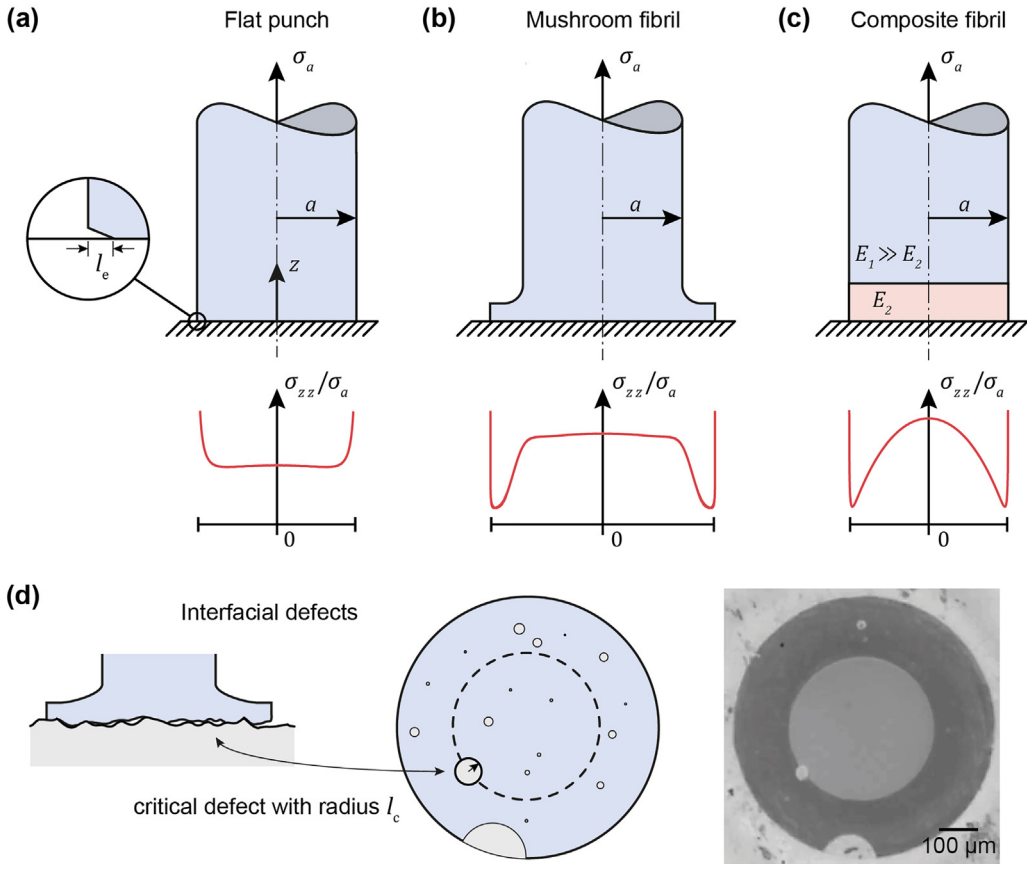

FIG. 1. Schematic of contact formation at a fibrillar micropatterned feature. (a)–(c) Axisymmetric designs of fibrillar sub-contacts with exemplary normalized interfacial stress distributions obtained by numerical simulations: (a) flat punch; (b) mushroom fibril; and (c) composite fibril. In (a), the detachment is considered by propagation of an edge defect with the length, l_e. (d) Realistic contact to a rough/contaminated surface that induces multiple interfacial defects.

strength at the intrinsic limit known as flaw-insensitivity.[36] However, the requisite feature size can prove challenging in fabrication. Accordingly, refined tip structures have been explored as an alternative means to mitigate contact edge stress concentrations. One common example is the so-called mushroom-tip fibril [Fig. 1(b), e.g., Refs. 29, and 37–39] with its thin flange region extending from the contact edge. This reduces the strain energy at the contact edge and creates a turning action when subject to tensile load, which can even lead to compressive stresses in this region,[20,40] ultimately decreasing the likelihood of edge defect propagation. Another is the bi-material soft-tip-layer (composite) fibril [Fig. 1(c), e.g., Refs. 41–43]. These exploit a confinement effect, which increases stress toward the center of the contact,[21,44,45] again reducing the propensity for edge defects to drive detachment. Qualitative descriptions of the tensile stress at the interface for each fibril design are shown in Figs. 1(a)–1(c).

Efforts have been made to obtain the strength absent consideration of preexisting defects, typically by cohesive zone modeling.[22,46,47] Defects nucleate in the region of highest interfacial stress, and the resulting strength is deterministic, in that it is controlled by the geometry of the fibril only. This is also true of the case where pre-existing defects are present, but suction effects are dominant and the pressure inside the cavity is negligible.[19]

B. Dependence upon interfacial defects

Interfacial defects, such as in Fig. 1(d), are omnipresent in real adhesive contacts and can result from different sources, as briefly discussed below:

- Surface roughness has a tremendous influence on adhesion and has been investigated extensively for decades.[48–50] Here, we will limit ourselves to a discussion of relevant length scales of the roughness. For more detailed information on roughness modeling, we refer the reader to the following article.[51] Roughness can exist over several decades of length scales and is not only limited to the counter surface but also can be introduced through the adhesive.[52,53] Roughness can impede the complete contact between the adhesive and the counter surface. At fine scales, the effective adhesion energy, W_{eff} and the adhesion strength, $\sigma_{\max}$ monotonically decrease due to an expanding mean gap at the interface, which reduces tractions.[54,55] This reduction is even stronger as the fractal dimension increases. At larger scales, elastic deformations become more effective and reduce the dependence on the mean gap.[50] Note that large scale defects can possibly exceed the transition flaw size, l_t, which then should be treated by a linear elastic fracture mechanics framework. This distinction is elaborated upon below and in Sec. V E.
- Contaminant residues comprise dust or wear particles, polymer/molecular thin films, and other species that locally alter the adhesive interaction.[56,57] For example, non-crosslinked pre-polymers and small amounts of silicone oils can reduce the adhesion during repeated tests of silicone elastomers.[56] Solid particles located in the interface usually reduce adhesion due to at least two reasons:[57] First, their adhesion to stiff counter surfaces is quite weak, and second, their presence causes additional elastic deformation resulting in reduced contact area. From the perspective of defect characterization, particles exhibit finite sizes while the dimensions of molecular thin films may be difficult to detect.
- Manufacturing atomically flat surfaces and perfect edges without fillets are nearly impossible, as each micropatterning technique bears limited resolution.[58,59] For example, micromachining and three-dimensional printing of templates for replica molding often result in rough surface finishes and defects. Furthermore, the combination of flexible molds with thermal expansion and shrinkage of polymers during curing can lead to inaccuracies of the final design.[60] Demolding from templates could further damage the final microstructure.

Overall, interfacial defects are defined as regions of the interface, where the separation exceeds the range of the adhesive interaction. They vary in size, location, distribution, and nature (including non-contacting areas, weakly adhering particles or organic thin films, and fabrication imperfections). With repeated contact of the adhesive and the target surface, defect locations and sizes may vary due to differences in positioning as well as wear and fouling.

Under the assumption of an ideally sharp penny-shaped defect, linear elastic fracture mechanics predicts the critical stress at which the defect will grow as[61]

$$\sigma_{\max} = \beta\sqrt{\frac{E^* W}{l_c}}, \tag{2}$$

where the radius of the defect is l_c. If the defect is small and located far from any geometric features such as the contact edge, then the factor β is a constant of order unity. Since the nominal stress experienced by the region in which the defect is located will depend upon the geometry of the fibril, as outlined in Sec. II A, β may depend upon l_c. Consequently, variation in the size and location can lead to statistical variation in strength. The observed strength will be related to a competition between various defects having different characters, and that which propagates at the lowest applied stress (associated with the lowest strength) will trigger detachment. Significantly, it has been shown that this effect may change the scaling of the strength with the characteristic sub-contact size, a.[59]

The preceding discussion raises the question of what constitutes a defect within the modeling framework of linear elastic fracture mechanics and thus, when an approach without assumption of a pre-existing defect might lead to valid predictions? The primary assumption is that the region close to the crack tip where rupture occurs, termed the "fracture process zone," is embedded within a stress field, which is accurately represented by the asymptotic elastic prediction.[62,63] In this case, the asymptotic elastic crack tip stress fields effectively control the details of failure inside the fracture process zone. For this to hold, the dimensions of the fracture process zone must be much smaller than that of the adhesive contact or the defect itself. The validity of the assumption of a small-scale fracture process zone must be assessed by estimating its size. Estimating the extent of the region over which the elastic stresses at the crack tip exceed the intrinsic strength, a characteristic length scale[36]

$$l_t \cong \frac{E^* W}{{\sigma_0}^2}, \tag{3}$$

emerges, where σ_0 is the intrinsic strength of the adhesive bond. Defects having characteristic size smaller than l_t will not initiate separation via propagation through the interface. If all defects within the contacting region are below this limit, then modeling approaches

based upon the assumption of no preexisting defects, as discussed in Sec. II A, should provide a valid result. Local detachment will be associated with nucleation of a defect of the region of highest interfacial stress, and the resulting strength will be deterministic. For a typical elastomeric fibril ($E^* \sim 2$ MPa) adhering to a glass substrate ($W \sim 50\,\mathrm{mJ/m^2}$, $\sigma_0 \sim 1$ MPa),[64] l_t is on the order of a few hundred nm, which is much smaller than the defects visible in Fig. 1(d).

C. *In situ* observation of sub-contacts and defect-controlled detachment

In situ observations often allow detection of the position of critical defects and their growth until detachment. Correlating these *in situ* observations of detachment with force–displacement measurements links micromechanical events to local and global adhesion measures and crucially allows for determination of the adhesive strength of each individual fibril.

Figure 2 shows the setup and results of such an experiment.[33] A micropatterned adhesive surface is brought into contact with a glass substrate [Fig. 2(a)] by normal approach, until a specified compressive preload is attained. The adhesive strength is then determined by normal retraction until the surfaces separate completely. The load and displacement are recorded throughout, and high contrast contact imaging is obtained by frustrated total internal reflection [Fig. 2(b)]. To determine the local adhesive strength of individual fibrils by correlation of the time of detachment with the global load or displacement, it is necessary to ensure that the load per fibril is uniform across the array. This is achieved with a sufficiently thin backing layer and a small array[65] and is verified by ensuring that there is neither a preference for detachment of fibrils close to the array perimeter nor any correlation between the detachment of one fibril and subsequent detachment of a neighbor.[32] It must also be verified that the load cell is sufficiently stiff so as not to trigger unstable detachment.[33] Under these conditions, deformation is dominated by fibril stretching. The critical

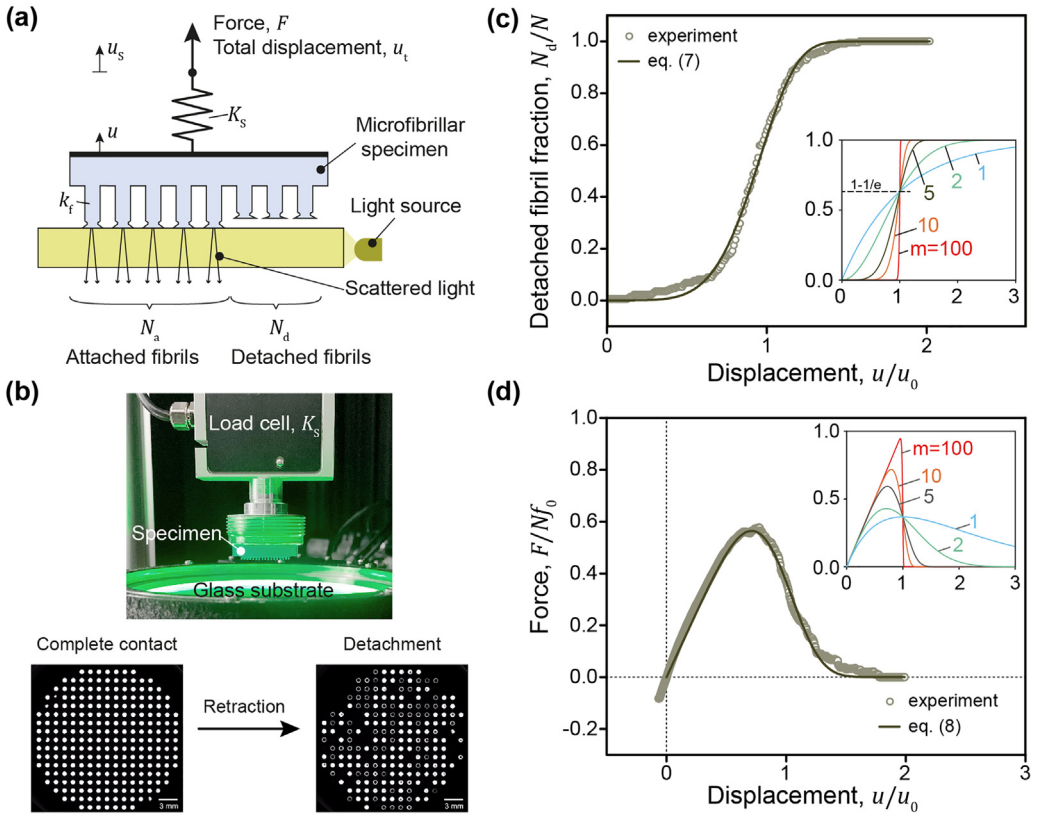

FIG. 2. Representative adhesion test of a micropatterned surface with *in situ* sub-contact visualization by frustrated total internal reflection. (a) Schematic of the adhesion setup described in Sec. II C. The microfibrillar adhesive (blue) adheres to a nominally flat glass substrate (yellow). The force F and the total displacement u_t are recorded during tests. The applied load is shared by the attached fibrils N_a, which individually have stiffness k_f. The spring attached in series with the microfibrillar adhesive represents the loading system stiffness K_s. The contrast between adhered and detached fibrils was enhanced by the principle frustrated total internal reflection, allowing N_a to be determined by *in situ* visualization using a camera positioned under the substrate. (b) Image of the experimental setup (left), as well as *in situ* observation of fibril contacts from below the substrate at preload (left) and during detachment (right). Light and dark areas represent contacting and non-contacting regions, respectively. (c) Fraction of fibrils detached from the substrate N_d/N vs normalized displacement u/u_0 (circles). The solid line corresponds to best fit using Eq. (7) with parameters m and u_0. The inset shows theoretical variations of N_d/N vs u/u_0 for Weibull moduli ranging from 1 (stochastic limit) to 100. (d) Normalized force F/Nf_0 vs normalized displacement u/u_0 obtained from adhesion tests (circles). The solid lines correspond to theoretical predictions given in Eq. (8). The inset shows characteristic force–displacement curves for Weibull moduli ranging from 1 to 100. Adapted from Ref. 33.

displacement at which a fibril detaches can be related to the critical force or critical stress as

$$u_{\max} = \frac{f_{\max}}{k_f} = \frac{\sigma_{\max} A_f}{k_f}, \tag{4}$$

where A_f is the cross-sectional area of the fibril stalk. Since k_f and A_f are unchanged from fibril to fibril, any of these three parameters ($u_{\max}$, $f_{\max}$, or $\sigma_{\max}$) can be used equivalently to characterize the local adhesive strength.

As the surfaces are separated, progressive detachment of fibrillar sub-contacts is observed [Fig. 2(b)], evidencing variation in the local adhesive strength. According to the discussion of Sec. II B, the observation that the strength varies suggests that the detachment is defect-controlled, and the critical defect size and character differ from fibril to fibril. The detached fibril fraction, N_d/N, vs displacement data u/u_0 [Fig. 2(c)] represents a cumulative statistical distribution function of the local adhesive strength (in the form of the critical displacement $u_{\max}$). We note that the normalization by u_0 is the result of the fitting by a Weibull distribution model, as discussed in Sec. III A.

III. CHARACTERIZATION OF STATISTICAL VARIATION IN SUB-CONTACT ADHESIVE STRENGTH

A. Single defect population

With data capturing the distribution of the local adhesive strength, efforts have been made to extract representative statistical parameters. This problem is similar to that encountered in characterizing the ultimate strength of bundles of threads and fiber-reinforced composites.[66–71]

The statistical theory of fracture is based upon the Poisson postulates. The assumption is that defects are highly dispersed within a critical region of the interface. This region may, in general, be a high-stress perimeter [as illustrated by the dashed line in Fig. 1(d)] or area. The number of critical defects in non-overlapping sections is assumed independent, the probability of a critical defect existing within a small increment of the region of interest is proportional to its size, dS, and the probability of multiple critical defects existing within this region is negligible. This is the basis of the derivation of the Poisson distribution[72]

$$\Phi(f, S) = 1 - \exp\left(-\int_f \int_S g(f, S)\mathrm{d}S\mathrm{d}f\right), \tag{5}$$

where Φ is the probability of detachment, f is the local tensile load applied to the fibril, and $g(f, S)$ is the number of defects per unit length of perimeter or area, which yield a fibril adhesive strength between f and $f + \mathrm{d}f$. The possibility of a non-uniform stress state in the critical region leads to the dependence of g on S. Weibull[73] assumed an empirical power-law form of this function on account of its simplicity and versatility in describing experimental trends, leading to

$$\Phi = 1 - \exp\left[-\frac{S}{S_0}\left(\frac{f}{f_0}\right)^m\right], \tag{6}$$

where S_0 is the reference fibril contact perimeter or area, f_0 is the reference value for the fibril adhesive strength, and m is the Weibull modulus. Although not exactly the arithmetic mean, the parameter f_0 is representative of the average strength of fibrillar sub-contacts. The parameter m is reflective of the variability in strength from fibril to fibril, with $m = 1$ being the stochastic lower bound and $m = \infty$ being the deterministic upper bound (i.e., the strength of all fibrils is identical). The dependence on S is reflective of the increased likelihood of there being a critical defect as the size of the critical high-stress region is increased. Moving forward, we will consider only an array of geometrically uniform fibrils, for which $S = S_0$, and the detachment probability simplifies to

$$\Phi = 1 - \exp\left[-\left(\frac{f}{f_0}\right)^m\right] = 1 - \exp\left[-\left(\frac{u}{u_0}\right)^m\right], \tag{7}$$

where the equivalent statement in terms of displacement is obtained via Eq. (4), where u_0 is the reference value for the critical displacement at detachment. The statistical properties u_0 and m can be extracted from experiment by recognizing that the detached fibril fraction, N_d/N, is exactly the normalized rank in strength from lowest to highest and is, therefore, equivalent to the detachment probability, Φ. Figure 2(c) shows representative experimental data in good agreement with Eq. (7).[33] The inset shows the theoretical trends of various m for the ideally Weibull-distributed adhesive strength.

B. Multiple defect populations

If critical defects emerge from two sources, as shown schematically in Fig. 1(d) and during detachment in Fig. 3, then fitting of Eq. (7) may still be performed but the resulting statistical properties will not be reflective of either population individually.[31] Edge defects have been found to result from fabrication imperfections and generally lead to a lower adhesive strength than the fibril-geometry and interfacial roughness-controlled center defects [Fig. 3(a)]. Consequently, a fibril detaching due to an edge defect possess center defects within the interface, which would have resulted in higher adhesive strengths. The loss of information about these defects distorts the emerging statistical properties of the center defect distribution.

Multiple defect populations may be addressed by the use of partially or fully concurrent statistical frameworks,[74] accounting for the fact that the probability of detachment must be the product of the probabilities of detachment due to each population individually. However, this approach lacks utility for fitting to experimental data as the resulting parameter space is extremely large. An alternative, if the detachment mechanism is known on a fibril-by-fibril basis, is to try to decouple the populations. The mean order ranking method[75] accounts for the position of the weaker population within the sequence (from low to high strength) to reflect the increased probability that the disguised strengths from the other population would have exceeded subsequent data. As shown in Fig. 3(b), this approach has been adopted to extract approximately decoupled statistical properties of edge and center defects in the aforementioned system.[31]

IV. EFFECT ON ADHESIVE PERFORMANCE OF MICROPATTERNED ARRAYS

A. Strength of attachment

In the first work to consider the global strength of an adhesive patch due to statistical variation in the strength of fibrillar sub-contacts,[30] Monte Carlo simulations were performed assuming a power law distributed strength and uniform load distribution across the

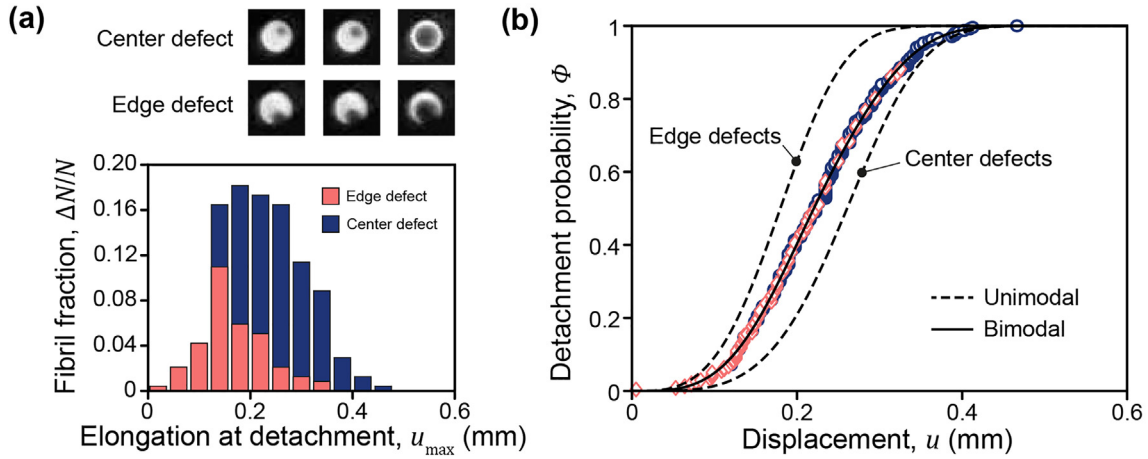

FIG. 3. Multiple defect populations. (a) Histogram of the fibril fraction with a given elongation at detachment, revealing the strength distribution decomposed by defect type—edge (red) and center defects (blue) as shown in contact images above the graph. (b) Detachment probability with experimental data points fitted to using a bimodal statistical model (solid line) to address edge and center defects. Dashed lines represent approximate unimodal models for decoupled distributions of edge and center defects. Adapted from Ref. 31.

fibril array. A monotonic decay in the global adhesive strength was revealed as the variability in local strength increased. Later, a closed form expression for the global strength was obtained using Weibull's statistical framework introduced in Sec. III A.[31] The load–displacement relationship (starting from full contact at $u = 0$ mm) is

$$F = Nk_f u \exp\left[-\left(\frac{u}{u_0}\right)^m\right]. \tag{8}$$

Figure 2 shows that, upon extraction of the statistical properties from the *in situ* visualization measurement [Fig. 2(c)], excellent agreement between this relationship and the experimental force–displacement characteristics is observed [Fig. 2(d)].

The load maxima yielded by differentiation of Eq. (8) provide the global adhesive force in terms of the statistical properties as

$$F_{max} = Nk_f u_0 \left(\frac{1}{m}\right)^{\frac{1}{m}} \exp\left(-\frac{1}{m}\right). \tag{9}$$

Normalization by the total size of the array then gives the global adhesive strength σ_p typically referred to as the pull-off strength.

An increase in the reference fibril adhesive strength results in a corresponding (linear) increase in the global adhesive strength. More significantly, reduction in the Weibull modulus (corresponding to an increase in the variability of the fibril adhesive strength) leads to a monotonic reduction in the global adhesive strength. This is a consequence of the detrimental impact of early detachments due to weak fibrils, which increase the share of load on fibrils which remain in contact. We further note that the area enclosed by the load–displacement curve corresponds to the work of separation. For the normalized curves shown in the inset of Fig. 2(d), the dimensionless work of separation, $W_s/Nk_f u_0^2$, varies between the limits of 0.5 and 1 for $m = \infty$ and $m = 1$, respectively. This suggests a possible benefit of variability in the local adhesive strength. Another is revealed in the section which follows.

B. Stability of attachment

In most applications, a stiffness component K_s is effectively added in series with that of the microfibril array [Fig. 2(a)]. Previous reports have shown that the variation of the system stiffness affects crack propagation rates during debonding and, more significantly, can induce a transition from stable to unstable crack growth leading to catastrophic failure of the adhesive contact.[76,77] During a detachment event, the load supported drops, and the increase in displacement of the adhesive is controlled by the ratio of the stiffness of the system to that of the adhesive itself. If this increase is too large (as it is for a compliant system) then further detachment events will be triggered, indicating the onset of an instability. The variability in the local adhesive strength controls the rate of detachment and, thus, the likelihood of causing further detachments [Fig. 2(c)]. The following stability criterion was obtained for fibrillar adhesives, exhibiting ideally Weibull distributed local strength[33]

$$\frac{K_s}{Nk_f} > m\exp\left[-\frac{1}{m}(1+m)\right]. \tag{10}$$

Figure 4 shows the stability map associated with Eq. (10). A narrow distribution in the fibril adhesive strength (high Weibull modulus), while providing a higher global strength, exhibits higher rates of detachment and, thus, requires a stiffer loading system to ensure stability throughout. Good agreement with experimental data is observed. This criterion can, therefore, inform the design of loading systems for the avoidance of unstable detachment in handling delicate objects.

V. FUTURE DIRECTIONS

A. Non-uniform load distribution among fibrils

The effects of non-uniform load distribution among fibrils due to elastic coupling by the backing layer, substrate curvature, or misalignment have been extensively modeled using semi-analytical approaches.[25,26,28] Considering the local adhesive strength based on a Weibull statistical distribution, a competition emerges between the

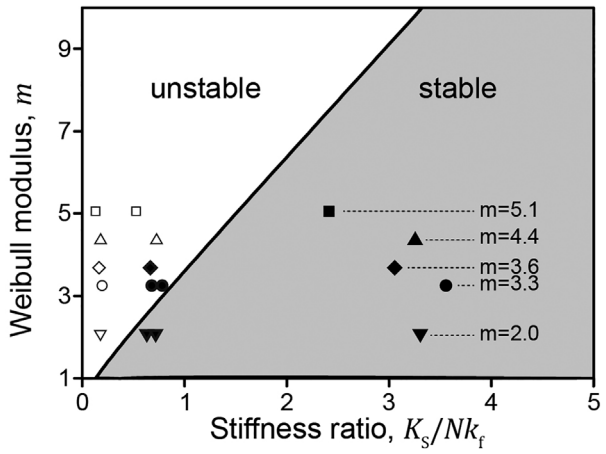

FIG. 4. Map to predict stable (gray region) and unstable (white region) detachment as a function of the Weibull modulus m and stiffness ratio K_s/Nk_f. The solid line separating both regimes is given in Eq. (10). Symbols represent experimental results for specimens with various Weibull moduli m, where full and open symbols correspond to stable and unstable detachment, respectively. Adapted from Ref. 33.

variability and load concentrations in controlling the global adhesive strength of the micropatterned array.[78] One example of this effect is depicted in Fig. 5. The backing layer compliance is varied by changing its thickness, H [Fig. 5(a)] with rigid ($H = 0$) and fully compliant ($H = \infty$) limits considered. Deterministic ($m = \infty$) and stochastic ($m = 5$) local adhesive strength is considered, when the load–displacement [Fig. 5(b)] and detachment characteristics are examined. In the deterministic case, the characteristic array edge load concentration, which results due to elastic coupling by the backing layer ($H = \infty$), controls the detachment process.[25] The strength is reduced as compared to a rigid backing layer ($H = 0$), for which the load distribution is uniform. In the stochastic case, detachments of weaker fibrils in random positions throughout the array are evident in combination with those at the array edge due to the load concentration. This further reduces the strength but crucially makes the difference between the rigid and compliant backing limits smaller. When the entire range of physically relevant Weibull moduli is explored [Fig. 5(c)], a convergence of the strength, independent of the backing layer properties and the associated load concentration, is observed when the variability in the local strength is large (low m). This suggests that the influence of load concentrations can be modulated by the statistical properties of the local adhesive strength. This is currently being investigated experimentally.

The modulation of load concentrations by statistical variability in the local strength could prove to be extremely significant in understanding the design and characterization of micropatterned adhesives. Load concentrations control the performance across length-scales and ultimately can necessitate hierarchical subdivision of micropatterned arrays.[79] The influence of statistical effects on this aspect of the design process should be considered. The effect of the array size on the local strength statistics themselves must also be investigated, as the former controls the effective sample size from which the distribution is drawn. Since experimental measurement systems can also include load concentrations (such as for a spherical probe), the ability to reliably extract representative performance metrics, when the local statistical variation in strength is exhibited, must also be considered.

B. Suction effects

Determining the adhesive strength of each individual fibril further provides the opportunity to provide physical insight on variations in the global adhesive strength of the micropatterned array. One such example is the observation of the reduced adhesion strength on the order of a few tens of percent upon reduction of the air pressure. This is significant for applications in vacuum chambers or in space. Suction forces are generated at the tips of individual fibrils and can only contribute to adhesion when center defects occur as the presence of an expanding cavity is required.[19] This excludes the flat punch geometry, which only detaches by propagation of edge defects. In contrast,

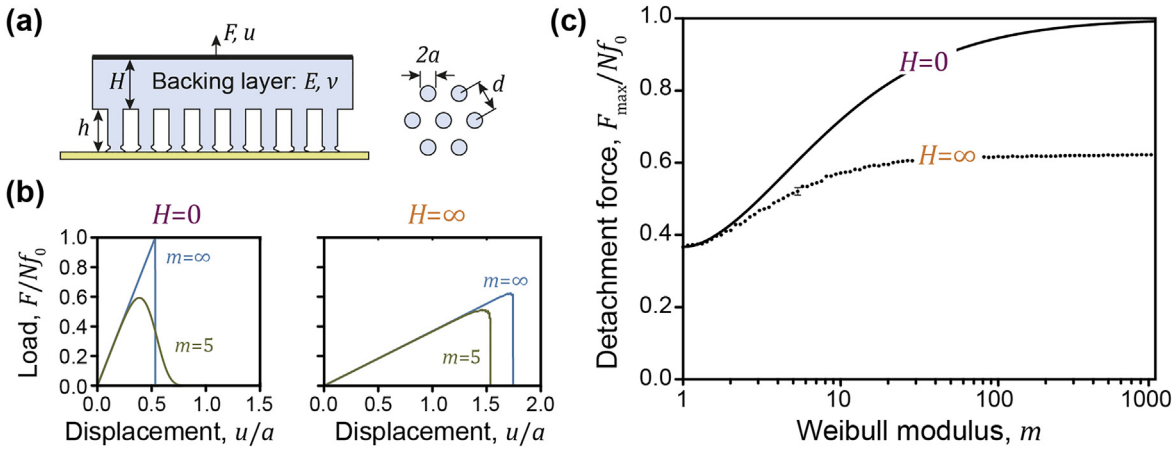

FIG. 5. Local strength statistics vs array-scale load distribution. (a) Schematic of an adhesive array with an elastic backing layer of thickness H, where h is the length of the fibril, E is Young's modulus, and ν is Poisson's ratio. (b) Model load–displacement curves for an adhesive with rigid (left, $H = 0$) and fully compliant (right, $H = \infty$) backing layer for two values of the Weibull modulus $m = 5$ (green) and $m = \infty$ (blue). (c) Normalized detachment force, F_{max}/Nf_0 vs Weibull modulus, m. The solid line represents the rigid backing layer ($H = 0$) corresponding to Eq. (9), whereas the dots correspond to the fully compliant backing layer ($H = \infty$). Adapted from Ref. 78.

mushroom fibrils, composite, and cupped microstructures are more likely to failure by center defects. Thus, to a first order approximation, the number of fibrils detaching via center defects could be assumed to play a decisive role in contributing to suction. However, Tinnemann *et al.*[32] have disproved this hypothesis, as experiments conducted on rougher surfaces resulted in a higher number of fibrils with center defects but a lower suction contribution. The authors suggest that this is due to increased leakage from cavities at the interface, which reduce the suction contribution. Overall, the contribution of suction to adhesion is sensitive to defects and percolation paths, which vary from fibril to fibril. Therefore, the statistical properties may vary for repeated attachments in different locations on the substrate.

C. Rate effects

The theoretical framework presented above is currently limited to linear elasticity. Rate effects associated with viscoelasticity are ignored. These should be implemented into the statistical models, considering bulk viscoelasticity associated with the elongation of the fibrils and the effective adhesion energy due to viscoelastic effects at the tip of interfacial defects. This will reveal whether statistical properties, such as the Weibull modulus, vary at different rates. This is significant, as the rate is easy to control in applications.

Another rate-dependent phenomenon is referred to as contact aging. Longer times in contact with the substrate lead to the reduction in defect sizes due to relaxation processes and the formation of chemical bonds across the interface. Both mechanisms increase the adhesion strength and may modify statistical properties. Thiemecke and Hensel[80] found that the reference elongation at detachment increased for long-term contacts (>60 s) due to the formation of new interfacial bonds. Clear trends for the Weibull modulus were not obtained, as similar specimens behaved differently. Short-term contacts (<60 s) also did not lead to clear trends in the resulting statistical measures, likely due to resolution limits in the detection of defect sizes when observing the entire adhesive array. In summary, mechanisms leading to defect healing and their influence on statistical properties are not yet fully understood.

D. Modeling fibril adhesive strength due to varied defect character

Existing studies of the fibril adhesive strength, as reviewed in Secs. II A and II B have considered an idealized and limited range of the interfacial defect size and position for each type of fibril design. Pre-existing defects have either been neglected[22,47] or have been considered only at the contact edge[20,21,35,40,46] or contact center.[19,81] This limits the ability to link the emerging statistical properties of the adhesive strength to the character of defects at the interface. Small defects centered in a seemingly critical region (e.g., at the contact center) may be less damaging than large defects in sub-critical regions. Defects have also been considered to have idealized shape, where the shape of non-contacting domains that emerge due to the surface roughness may be quite different and play a role in the strength of attachment. Given the extensive parameter space of the problem (encompassing fibril design as well as defect character) and the computational cost of simulations, machine learning models trained using simulation results could prove to be an effective tool (as demonstrated for the task of optimizing fibril design).[82,83]

E. Modeling and characterization of interfacial defect formation

Understanding the local adhesive strength, which emerges due to differing defect characters, is necessary, but insufficient alone to provide predictive capabilities of performance. This requires an understanding of how the defects, specifically non-contacting regions exceeding the transition flaw size of Eq. (3), emerge given the characteristic properties of imperfections and surface roughnesses at the interface. Modeling efforts should reveal the characteristic size, shape, and distribution of defects within the interface as a function of the surface power spectral density (PSD), bulk material properties, and applied preload.

Models derived from such activities require experimental validation based on microscopic defect detection, which requires imaging methods exhibiting large contrasts between attached and detached regions. Potential methods comprise frustrated total internal reflection, dark field imaging, fluorescence microscopy, imaging ellipsometry, and so on, which provide spatial information and access to determine size distributions. Alternative strategies for non-transparent solids include acoustic microscopes or computer tomography.[84]

F. AI-assisted modeling based on contact images

An attractive approach to overcome the complexity of modeling adhesive contacts with defects is the combination of *in situ* detection of defects and artificial intelligence (AI) trained systems such as machine learning algorithms and deep learning networks. It was recently demonstrated that adhesion can be predicted by supervised machine learning.[85] Several features were obtained from contact images on the fibrillar level and fed into regression models. The trained models enabled high precision prediction of adhesion for partial contacts due to misalignments. Such a near real-time processing is of high practical relevance, since it can be easily implemented into pick-and-place grippers for in-line evaluation of whether an object can be reliably grasped.

Moreover, existing physical models can potentially be extended by data-driven flexible models to account for complex and variable defect constellations (e.g., due to roughness or irregular shapes of fibrils and arrays).[86] Such hybrid algorithms use differentiable instances of known physical models to estimate unknown parameters or parameterizable experimental variations. Such architectures have been successfully implemented to learn residual physical components of multiple models related to throwing,[87] cutting,[88] and friction dynamics.[89]

VI. SUMMARY

In this Perspective, we reviewed the current understanding of multiscale contact mechanics in the problem of biologically inspired micropatterned adhesives. In particular, we have addressed the importance of introducing statistical frameworks to account for local variation in the adhesive strength, leading to a paradigm shift in the understanding of global performance. This new direction has been motivated by recent experiments, in which defect-controlled detachments of fibrils were observed and distributions of the adhesive strength in fibril arrays were determined. Variation in defect size and location across the array determines the statistical properties, which, in turn, influence the overall performance of the adhesive. We explored

the detachment probability for both single or multiple defect populations, the load–displacement relationships that emerge from Weibull statistics, and a stability criterion for preventing sudden detachments. Finally, we outlined potential future directions that extend existing models by consideration of non-uniform loading and rate effects. Another open issue highlighted is the determination of critical defect characteristics responsible for the detachment of each fibrillar contact. Along with the experimental challenge of determining the size and shape of defects, modeling the adhesive strength controlled by formation of non-idealized defects on rough and contaminated surfaces is necessary.

ACKNOWLEDGMENTS

R.H. acknowledges funding by the Leibniz Competition Grant MUSIGAND (No. K279/2019).

AUTHOR DECLARATIONS

Conflict of Interest

Authors declare no conflict of interest.

DATA AVAILABILITY

The data that support the findings of this study are available from the corresponding authors upon reasonable request.

REFERENCES

[1]E. Arzt, H. Quan, R. M. McMeeking, and R. Hensel, Prog. Mater. Sci. **120**, 100823 (2021).
[2]R. G. Beutel and S. N. Gorb, J. Zool. Syst. Evol. Res. **39**, 177 (2001).
[3]W. Federle, J. Exp. Biol. **209**, 2611 (2006).
[4]A. Y. Stark, I. Badge, N. A. Wucinich, T. W. Sullivan, P. H. Niewiarowski, and A. Dhinojwala, Proc. Natl. Acad. Sci. **110**, 6340 (2013).
[5]E. Arzt, S. Gorb, and R. Spolenak, Proc. Natl. Acad. Sci. **100**, 10603 (2003).
[6]T. Tang, C.-Y. Hui, and N. J. Glassmaker, J. R. Soc. Interface **2**, 505 (2005).
[7]C.-Y. Hui, N. J. Glassmaker, T. Tang, and A. Jagota, J. R. Soc. Interface **1**, 35 (2004).
[8]M. Kamperman, E. Kroner, A. del Campo, R. M. McMeeking, and E. Arzt, Adv. Eng. Mater. **12**, 335 (2010).
[9]R. Hensel, K. Moh, and E. Arzt, Adv. Funct. Mater. **28**, 1800865 (2018).
[10]S. Song, D.-M. Drotlef, C. Majidi, and M. Sitti, Proc. Natl. Acad. Sci. **114**, E4344 (2017).
[11]S. N. Gorb, M. Sinha, A. Peressadko, K. A. Daltorio, and R. D. Quinn, Bioinspiration Biomimetics **2**, S117 (2007).
[12]E. W. Hawkes, E. V. Eason, A. T. Asbeck, and M. R. Cutkosky, IEEE/ASME Trans. Mechatronics **18**, 518 (2013).
[13]I. Hwang, H. N. Kim, M. Seong, S.-H. Lee, M. Kang, H. Yi, W. G. Bae, M. K. Kwak, and H. E. Jeong, Adv. Healthcare Mater. **7**, e1800275 (2018).
[14]G. Moreira Lana, K. Sorg, G. I. Wenzel, D. Hecker, R. Hensel, B. Schick, K. Kruttwig, and E. Arzt, Adv. NanoBiomed Res. **1**, 2100057 (2021).
[15]Y. Wang, V. Kang, E. Arzt, W. Federle, and R. Hensel, ACS Appl. Mater. Interfaces **11**, 26483 (2019).
[16]Y. Wang and R. Hensel, Adv. Funct. Mater. **31**, 2101787 (2021).
[17]C.-Y. Hui, A. Jagota, L. Shen, A. Rajan, N. Glassmaker, and T. Tang, J. Adhes. Sci. Technol. **21**, 1259 (2007).
[18]C.-Y. Hui, N. J. Glassmaker, and A. Jagota, J. Adhes. **81**, 699 (2005).
[19]M. Areyano, J. A. Booth, D. Brouwer, L. F. Gockowski, M. T. Valentine, and R. M. McMeeking, J. Appl. Mech. **88**, 031017 (2021).
[20]A. V. V. Spuskanyuk, R. M. M. McMeeking, V. S. S. Deshpande, and E. Arzt, Acta Biomater. **4**, 1669 (2008).
[21]R. G. Balijepalli, S. C. L. Fischer, R. Hensel, R. M. McMeeking, and E. Arzt, J. Mech. Phys. Solids **99**, 357 (2017).
[22]X. Zhang, Y. Wang, R. Hensel, and E. Arzt, J. Appl. Mech. **88**, 031015 (2021).
[23]F. H. Benvidi and M. Bacca, J. Appl. Mech. **88**, 121007 (2021).
[24]H. Khungura and M. Bacca, J. Appl. Mech. **88**, 031004 (2021).
[25]M. Bacca, J. A. Booth, K. L. Turner, and R. M. McMeeking, J. Mech. Phys. Solids **96**, 428 (2016).
[26]J. A. Booth, M. Bacca, R. M. McMeeking, and K. L. Foster, Adv. Mater. Interfaces **5**, 1800272 (2018).
[27]H. Khungura and M. Bacca, Mech. Mater. **160**, 103914 (2021).
[28]S. Bettscheider, D. Yu, K. L. Foster, R. M. McMeeking, E. Arzt, R. Hensel, and J. A. Booth, J. Mech. Phys. Solids **150**, 104365 (2021).
[29]L. Heepe, L. Xue, and S. N. Gorb, *Bio-Inspired Structured Adhesives: Biological Prototypes, Fabrication, Tribological Properties, Contact Mechanics, and Novel Concepts* (Springer, 2017).
[30]P. K. Porwal and C. Y. Hui, J. R. Soc. Interface **5**, 441 (2008).
[31]J. A. Booth, V. Tinnemann, R. Hensel, E. Arzt, R. M. McMeeking, and K. L. Foster, J. R. Soc. Interface **16**, 20190239 (2019).
[32]V. Tinnemann, L. Hernández, S. C. L. Fischer, E. Arzt, R. Bennewitz, and R. Hensel, Adv. Funct. Mater. **29**, 1807713 (2019).
[33]R. Hensel, J. Thiemecke, and J. A. Booth, ACS Appl. Mater. Interfaces **13**, 19422 (2021).
[34]K. Kendall, J. Phys. D **4**, 1186 (1971).
[35]S. N. Khaderi, N. A. Fleck, E. Arzt, and R. M. McMeeking, J. Mech. Phys. Solids **75**, 159 (2015).
[36]H. Gao and H. Yao, Proc. Natl. Acad. Sci. U. S. A. **101**, 7851 (2004).
[37]S. N. Gorb and M. Varenberg, J. Adhes. Sci. Technol. **21**, 1175 (2007).
[38]A. Del Campo, C. Greiner, I. Álvarez, and E. Arzt, Adv. Mater. **19**, 1973 (2007).
[39]S. Kim and M. Sitti, Appl. Phys. Lett. **89**, 261911 (2006).
[40]R. G. Balijepalli, M. R. Begley, N. A. Fleck, R. M. McMeeking, and E. Arzt, Int. J. Solids Struct. **85–86**, 160 (2016).
[41]H. K. Minsky and K. T. Turner, Appl. Phys. Lett. **106**, 201604 (2015).
[42]H. K. Minsky and K. T. Turner, ACS Appl. Mater. Interfaces **9**, 18322 (2017).
[43]S. C. L. Fischer, E. Arzt, and R. Hensel, ACS Appl. Mater. Interfaces **9**, 1036 (2017).
[44]M. Samri, A. Kossa, and R. Hensel, J. Appl. Mech. **88**, 031009 (2021).
[45]R. Hensel, R. M. McMeeking, and A. Kossa, J. Adhes. **95**, 44 (2019).
[46]N. A. Fleck, S. N. Khaderi, R. M. McMeeking, and E. Arzt, J. Mech. Phys. Solids **101**, 30 (2017).
[47]B. Aksak, K. Sahin, and M. Sitti, Beilstein J. Nanotechnol. **5**, 630 (2014).
[48]L. Pastewka and M. O. Robbins, Proc. Natl. Acad. Sci. **111**, 3298 (2014).
[49]A. Wang, Y. Zhou, and M. H. Müser, Lubricants **9**, 17 (2021).
[50]J. Joe, M. D. Thouless, and J. R. Barber, J. Mech. Phys. Solids **118**, 365 (2018).
[51]M. H. Müser, W. B. Dapp, R. Bugnicourt, P. Sainsot, N. Lesaffre, T. A. Lubrecht, B. N. J. Persson, K. Harris, A. Bennett, K. Schulze, S. Rohde, P. Ifju, W. G. Sawyer, T. Angelini, H. Ashtari Esfahani, M. Kadkhodaei, S. Akbarzadeh, J. J. Wu, G. Vorlaufer, A. Vernes, S. Solhjoo, A. I. Vakis, R. L. Jackson, Y. Xu, J. Streator, A. Rostami, D. Dini, S. Medina, G. Carbone, F. Bottiglione, L. Afferrante, J. Monti, L. Pastewka, M. O. Robbins, and J. A. Greenwood, Tribol. Lett. **65**, 118 (2017).
[52]B. B. Mandelbrot, D. E. Passoja, and A. J. Paullay, Nature **308**, 721 (1984).
[53]B. N. J. Persson, J. Chem. Phys. **115**, 3840 (2001).
[54]J. Joe, M. Scaraggi, and J. R. Barber, Tribol. Int. **111**, 52 (2017).
[55]B. N. J. Persson and M. Scaraggi, J. Chem. Phys. **141**, 124701 (2014).
[56]E. Kroner, R. Maboudian, and E. Arzt, IOP Conf. Ser.: Mater. Sci. Eng. **5**, 12004 (2009).
[57]Y. Mengüç, M. Röhrig, U. Abusomwan, H. Hölscher, and M. Sitti, J. R. Soc. Interface **11**, 20131205 (2014).
[58]P. Rivero, A. Simaite, and M. Spenko, Aerotec., Missili Spazio **98**, 187 (2019).
[59]R. M. McMeeking, E. Arzt, and A. G. Evans, J. Adhes. **84**, 675 (2008).
[60]D. Yu, D. Beckelmann, M. Opsölder, B. Schäfer, K. Moh, R. Hensel, P. de Oliveira, and E. Arzt, Materials (Basel) **12**, 97 (2018).
[61]M. K. Kassir and A. M. Bregman, J. Appl. Mech. **39**, 308 (1972).
[62]I. N. Sneddon, Proc. R. Soc. London, Ser. A **187**, 229 (1946).
[63]J. R. Rice, J. Appl. Mech. **55**, 98 (1988).
[64]T. Tang, A. Jagota, M. K. Chaudhury, and C.-Y. Hui, J. Adhes. **82**, 671 (2006).
[65]R. Long, C.-Y. Hui, S. Kim, and M. Sitti, J. Appl. Phys. **104**, 044301 (2008).
[66]H. E. Daniels and H. Jeffreys, Proc. R. Soc. London, Ser. A **183**, 405 (1945).
[67]S. J. Zhou and W. A. Curtin, Acta Metall. Mater. **43**, 3093 (1995).

[68]W. A. Curtin and N. Takeda, J. Compos. Mater. **32**, 2042 (1998).
[69]Z. Chi, T.-W. Chou, and G. Shen, J. Mater. Sci. **19**, 3319 (1984).
[70]M. R'Mili, Compos. Sci. Technol. **56**, 831 (1996).
[71]M.-H. Berger and D. Jeulin, J. Mater. Sci. **38**, 2913 (2003).
[72]B. W. Lindgren and G. W. McElrath, *Introduction to Probability and Statistics*, 3rd ed. (MacMillan Publishing Company, 1969).
[73]W. Weibull, *A Statistical Theory of the Strength of Materials* (Generalstabens litografiska anstalts förlag, Stockholm, 1939).
[74]C. Johnson, Stat. Microcracking **76**, 2117e20 (1981).
[75]L. G. Johnson, *Statistical Treatment of Fatigue Experiments* (Elsevier Science Ltd, 1964).
[76]M. Barquins, J. Appl. Polym. Sci. **28**, 2647 (1983).
[77]A. R. Mojdehi, D. P. Holmes, and D. A. Dillard, Soft Matter **13**, 7529 (2017).
[78]J. A. Booth, *Multiscale Mechanics of Bioinspired Dry Adhesives* (University of California Santa Barbara, 2019).
[79]H. Yao and H. Gao, J. Mech. Phys. Solids **54**, 1120 (2006).
[80]J. Thiemecke and R. Hensel, Adv. Funct. Mater. **30**, 2005826 (2020).
[81]L. Afferrante and G. Carbone, Macromol. React. Eng. **7**, 609 (2013).
[82]Y. Kim, C. Yang, Y. Kim, G. X. Gu, and S. Ryu, ACS Appl. Mater. Interfaces **12**, 24458 (2020).
[83]D. Son, V. Liimatainen, and M. Sitti, Small **17**, 2102867 (2021).
[84]F. Bertocci, A. Grandoni, and T. Djuric-Rissner, Sensors **19**, 4868 (2019).
[85]M. Samri, J. Thiemecke, E. Prinz, T. Dahmen, R. Hensel, and E. Arzt "Predicting the gripping performance of micropatterned adhesives using supervised machine learning." (submitted).
[86]E. Heiden, D. Millard, E. Coumans, Y. Sheng, and G. S. Sukhatme, arXiv:2011.04217 (2020).
[87]A. Zeng, S. Song, J. Lee, A. Rodriguez, and T. Funkhouser, IEEE Trans. Rob. **36**, 1307 (2020).
[88]E. Heiden, M. Macklin, Y. Narang, D. Fox, A. Garg, and F. Ramos, arXiv:2105.12244 (2021).
[89]S. Pfrommer, M. Halm, and M. Posa, arXiv:2009.11193 (2020).